Effects of Interfacial Interactions on Electrocatalytic Activity of Cytochrome *c* Oxidase in Biomimetic Lipid Membranes on Gold Electrodes

Masaru Kato,[a,b]* *Ryoya Sano,*[b] *Narumi Yoshida,*[b] *Masatoshi Iwafuji,*[b] *Yoshito Nishiyama,*[b] *Sayuki Oka,*[b] *Kyoko Shinzawa-Itoh,*[c] *Yuya Nishida,*[d] *Yasunori Shintani,*[d] *Ichizo Yagi*[a,b]*

[a] Faculty of Environmental Earth Science, Hokkaido University, N10W5, Kita-ku, Sapporo 060-0810, Japan.

[b]Graduate School of Environmental Science, Hokkaido University, N10W5, Kita-ku, Sapporo 060-0810, Japan.

[c]Graduate School of Science, University of Hyogo, Ako, Hyogo, Japan.

[d]Department of Molecular Pharmacology, National Cerebral and Cardiovascular Center, Suita, Osaka, Japan.

AUTHOR INFORMATION

Corresponding Authors

*masaru.kato@ees.hokudai.ac.jp (MK). *iyagi@ees.hokudai.ac.jp (IY)

ABSTRACT. Effects of interfacial interactions on the electrocatalytic activity of protein-tethered bilayer lipid membranes (ptBLMs) containing cytochrome *c* oxidase (C*c*O) for the oxygen reduction reaction are studied by using protein film electrochemistry and surface-enhanced infrared absorption (SEIRA) spectroscopy. Mammalian C*c*O was immobilized on a gold electrode *via* self-assembled monolayers (SAMs) of mixed alkanethiols. The protein orientation on the electrode is controlled by SAM–C*c*O interactions and is critical to the cytochrome *c* (cyt *c*) binding. The C*c*O-phospholipid and C*c*O-cyt *c* interactions modulate the electrocatalytic activity of C*c*O and more densely packed ptBLMs show higher electrocatalytic activity. Our study indicates that spectroscopic and electrochemical studies of ptBLMs can provide insights into the effects of relatively weak protein-protein and protein-lipid interactions on the enzymatic activity of transmembrane enzymes.

TOC GRAPHICS

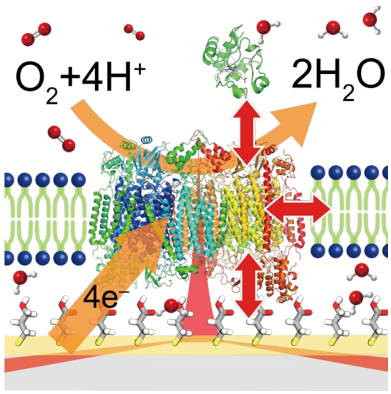

KEYWORDS. Protein–protein interactions, protein–lipid interactions, surface-enhanced infrared absorption spectroscopy, protein-tethered bilayer lipid membrane, protein film electrochemistry, oxygen reduction reaction.

TEXT.

In the mitochondrial respiratory chain, the stepwise electron transfer occurs from nicotinamide adenine dinucleotide (NADH), which can be generated from the food we eat, to oxygen, which can be taken from the air we breathe, between three major transmembrane protein complexes: complexes I, III and IV. The dysfunction of this electron transfer chain including a lack of electronic communication between protein complexes can cause mitochondrial disease.[1-4] The functionality of the transmembrane protein complexes can be modulated by relatively weak interactions at protein–protein[1-2,5-6] and protein–lipid[7-8] interfaces. Fundamental studies of impacts of such weak interactions on the enzymatic activity and intermolecular electron transfer would allow us to understand mechanistic insights into the dysfunction of the respiratory chain.

Complex IV, which is also known as cytochrome *c* oxidase (C*c*O), receives electrons from Complex III *via* a natural electron shuttle of cytochrome *c* (cyt *c*) and then reduces oxygen to water at the terminal respiratory chain.[6,9] The oxygen reduction reaction (ORR) catalyzed by C*c*O is coupled with pumping protons across the mitochondrial inner membrane, and then the proton motive force that is produced across the membrane drives the ATP synthesis by the ATP synthase. The enzymatic activity of C*c*O has been studied not only *in vivo* but also *in vitro*. For example, protein film electrochemistry (PFE) is an emerging technique to understand the redox behavior and enzymatic activity of redox proteins, where thin films of redox proteins are prepared on the surface of an electrode and then applying potentials to them initiates redox reactions of the proteins immobilized.[10-14] PFE can be coupled with surface-sensitive spectroscopic techniques such as surface-enhanced infrared absorption (SEIRA) spectroscopy, allowing us to understand the enzymatic activity, conformational changes, and protein–protein and protein–lipid interactions of redox enzymes including transmembrane proteins at the electrolyte–electrode interface.[15-19]

In this work, to quantitatively understand effects of protein interfacial interactions on the C*c*O enzymatic activity, we prepared protein-tethered bilayer lipid membranes (ptBLMs) of bovine C*c*O with phospholipids on SEIRA-active gold electrodes and then performed SEIRA spectroscopy and protein film electrochemistry of the ptBLMs in the presence or absence of the cyt *c* (**Figure 1**). Bovine C*c*O was immobilized on the gold surface *via* self-assembled monolayers (SAMs) of mixed alkanethiols of 3-mercaptopropionic acid (MPA) and 3-mercapto-1-propanol (MPL), which are terminated with carboxylate and hydroxyl groups, respectively. SAM–protein interactions can control the protein orientation of C*c*O on the electrode. The ptBLMs of C*c*O were reconstituted with phospholipids of 1,2-dimyristoyl-sn-glycero-3-phosphocholine (DMPC) or 1,2-dipalmitoyl-sn-glycero-3-phosphocholine (DPPC), which have different alkyl chain lengths, to understand the effect of lipid–protein interactions on the C*c*O activity for the ORR in the ptBLM. Then, cyt *c* was attached to ptBLMs to investigate effects of the protein–protein interactions on the ORR activity.

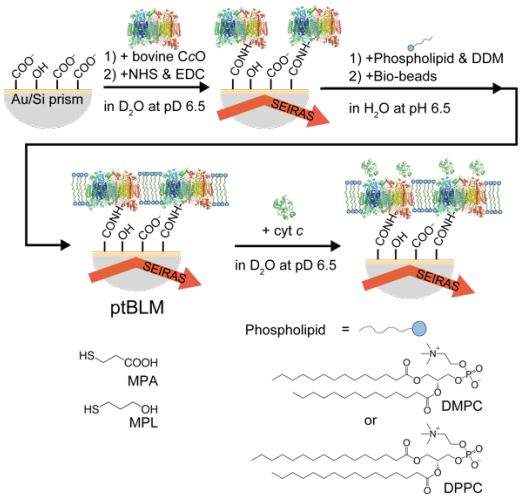

Figure 1. Schematic representation of immobilization of bovine C*c*O on a SAM on a SEIRA-active Au electrode, preparation of a ptBLM with a phospholipid of DMPC or DPPC, and cyt *c* binding to the ptBLM.

SEIRA-active Au films on half-cylindrical Si prisms were coated with mixed SAMs of alkanethiols with a 1:3 or 3:1 molar ratio of MPA–MPL (**Figure 1**). Since thiol groups react with the Au surface and terminal hydroxyl (-OH) and carboxylate ($-COO^-$) groups are exposed to the electrolyte solution, changing the molar ratio of MPA:MPL allows us to change the distribution of the protein orientation of C*c*O immobilized on the mixed SAM.[14] The carboxylate group of MPA is able to react with surface residues of lysine on C*c*O in the presence of amido coupling reagents of NHS and EDC [12]. Surface-exposed lysine residues can be mainly found on the protein surface exposed to the inside and outside of the mitochondrial inner membrane.[9] Similar protein immobilization methods have been used for large oxidoreductase proteins including transmembrane proteins.[12,17,20-21] In the following text, the mixed SAMs of 1:3 and 3:1 MPA–MPL are denoted as SAM_{OH} and SAM_{COOH}, respectively.

The surface immobilization of C*c*O on SAM_{OH} or SAM_{COOH} was tracked by SEIRA spectroscopy (**Figure 2**). Positive bands were observed at 1650 and 1460 cm^{-1}, which can be assigned to amide I' and amide II' bands in D_2O, respectively.[22] These band intensities increased over time and remained even after the gold surface was rinsed. Thus, C*c*O was successfully immobilized on either SAM_{OH} and SAM_{COOH}-modified Au surfaces.

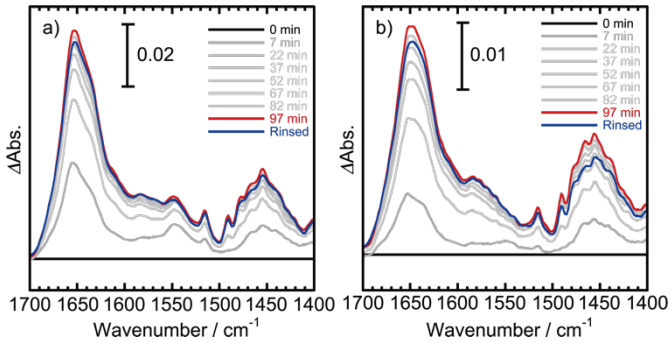

Figure 2. SEIRA spectral changes during the C*c*O immobilization on the mixed SAM of (a) SAM_{COOH} and (b) SAM_{OH} recorded in a 50 mM phosphate-buffered D_2O at pD 6.5. A polarization-

modulated SEIRA spectrum recorded in the phosphate-buffered D_2O solution containing no C*c*O was used as the reference spectrum (t = 0 min).

Peak intensity ratios of amide I' to amide II' in D_2O ($\Delta I_{\text{amide I'}}/\Delta I_{\text{amide II'}}$) in **Figure 2** were determined to be 2.6 and 2.2 for SAM_{COOH} and SAM_{OH}, respectively. These values are higher than that of C*c*O in solution (approximately 1.7).[23] SEIRA spectroscopy has a surface selection rule: vibrational modes with dipole moment perpendicular to the SEIRA-active surface are strongly enhanced whereas those parallel to the surface are weakened.[24] Furthermore, the amide I' mode of the α-helix is parallel to the helix axis whereas the amide II' mode is perpendicular to it.[22,25] The mammalian C*c*O is composed of 13 subunits and has 22 transmembrane helices in Subunits I, II, III, and IV-1 (Subunit I: 12 transmembrane helices; Subunit II: 2; Subunit III: 7; Subunit IV-1: 1).[9,26] Thus, transmembrane helices of the C*c*O either on SAM_{COOH}/Au or SAM_{OH}/Au adopt a more upright orientation (vertical to the Au surface). More details on the protein orientation of C*c*O on each SAM are discussed later with SEIRA spectra of the cyt *c* binding to C*c*O.

The BLM of DMPC (BLM_{DMPC}) was formed on C*c*O/SAM_{COOH}/Au or C*c*O/SAM_{OH}/Au. DMPC was dissolved in the phosphate-buffered solution (pH 6.5) containing a surfactant of DDM and the addition of bio-beads, which adsorb and remove DDM, initiated the formation of the BLM.[15-16,27] The formation process of BLM_{DMPC} was tracked by SEIRA spectroscopy (**Figure 3**). A negative band increased from 3000 to 3700 cm^{-1} and can be assigned to the OH stretching mode, ν(OH).[28] Two positive bands were observed from 2840 to 2870 cm^{-1} and from 2910 to 2940 cm^{-1} and can be assigned to the symmetric and asymmetric stretching modes, $\nu_s(CH_2)$ and $\nu_{as}(CH_2)$,

respectively.[15,17] The peak position of $\nu_{as}(CH_2)$ was found at 2923 cm^{-1}. These results indicate that the ptBLM of the C*c*O formed on either SAM_{COOH}/Au or SAM_{OH}/Au.

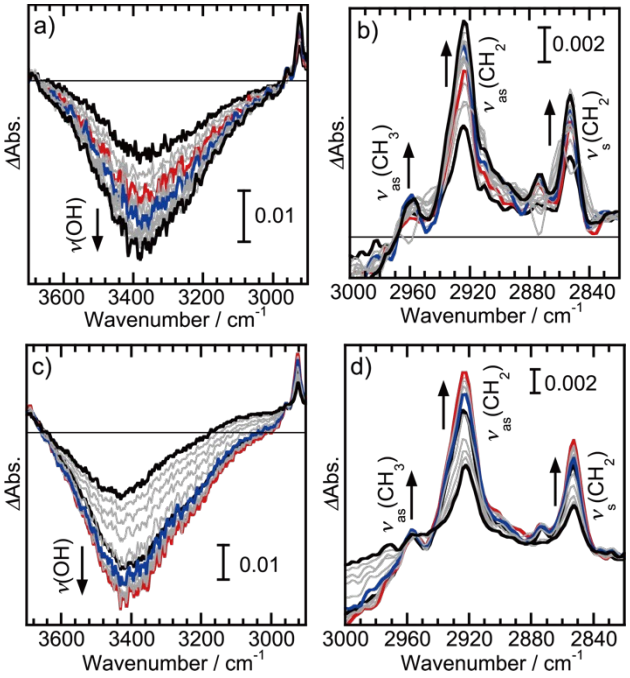

Figure 3. SEIRA spectral changes during the BLM_{DMPC} formation on (a,b) C*c*O/SAM_{COOH}/Au and (c,d) C*c*O/SAM_{OH}/Au recorded in a 50 mM phosphate-buffered solution (pH 6.5). A polarization-modulated SEIRA spectrum recorded just after the addition of DMPC solution at t = 0 min was used as the reference spectrum. For (a,b), the SEIRA spectra in black indicate the spectra at t = 22 and 247 min. For (c,d), the SEIRA spectra in black indicate the spectra at t = 22 and 187 min. The SEIRA spectra in red and blue show the spectra at t = 67 and 112 min after the addition of bio-beads at t = 60 and 100 min, respectively.

The binding processes of cyt *c* to the $ptBLM_{DMPC}$ on SAM_{COOH} and SAM_{OH} was tracked by SEIRA spectroscopy and the enzymatic activity of C*c*O before and after the cyt *c* biding was checked by cyclic voltammetry (**Figure 4**). After the addition of cyt *c* in the 50 mM phosphate-buffered D_2O solution, amide I' and II' bands positively increased for SAM_{COOH} whereas a marginal increase was observed for SAM_{OH} (**Figure 4a** and **4b**). These bands were still observed even after rinsing the surface with the buffered solution for SAM_{COOH} whereas these bands

disappeared and the same spectrum as the initial one was observed for SAM_{OH}. For control experiments, the cyt *c* binding processes to C*c*O/SAM_{COOH} and C*c*O/SAM_{OH} in the absence of BLM was also tracked (See **Figures S1** and **S2** in Supporting Information). Since the bands remained even after rinsing the surface with the buffered solution, we confirmed that cyt *c* was attached to either C*c*O/SAM_{COOH} or C*c*O/SAM_{OH} in the absence of BLM. These results indicate that cyt *c* binds to C*c*O on SAM_{COOH} but not on SAM_{OH} in the presence of BLM_{DMPC}. In the case of ptBLM_{DMPC}/SAM_{OH}, the cyt *c* binding site of C*c*O is directed toward the electrode substrate and covered with the BLM_{DMPC}, resulting in the inhibition of the access of cyt *c* to the binding site of C*c*O. In contrast, the cyt *c* binding site of C*c*O is directed toward the solution on SAM_{COOH} and exposed to the solution even after ptBLM_{DMPC} formation, allowing for the cyt *c* binding.[11,14]

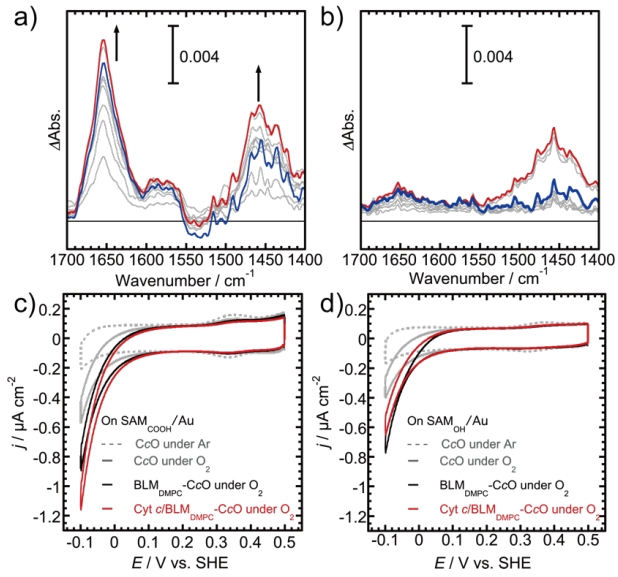

Figure 4. SEIRA spectral changes during cyt *c* binding to (a) BLM_{DMPC}-C*c*O/SAM_{COOH}/Au and (b) BLM_{DMPC}-C*c*O/SAM_{OH}/Au recorded in a 50 mM phosphate-buffered D_2O solution (pD 6.5). A polarization-modulated SEIRA spectrum recorded in the phosphate-buffered D_2O solution before the addition of cyt *c* was used as the reference spectrum (t = 0 min). The SEIRA spectra in red indicate the spectra recorded at t =127 min. The SEIRA spectra in blue indicate the spectra collected after rinsing the electrode surface with the buffered solution. CVs recorded at 10 mV s^{-1} in 50 mM phosphate buffered aqueous solution (pH 6.5) for (c) BLM_{DMPC}-C*c*O/SAM_{COOH}/Au and (d) BLM_{DMPC}-C*c*O/SAM_{OH}/Au before and after the cyt *c* binding. The electrodes were

prepared step by step as follows: C*c*O/SAM_{COOH}/Au, BLM_{DMPC}-C*c*O/SAM_{COOH}/Au and then cyt *c*/BLM_{DMPC}-C*c*O/SAM_{COOH}/Au for (c); C*c*O/SAM_{OH}/Au, BLM_{DMPC}-C*c*O/SAM_{OH}/Au and then cyt *c*/BLM_{DMPC}-C*c*O/SAM_{OH}/Au for (d).

We also constructed a BLM of DMPC on SAM_{COOH} in the absence of C*c*O and tracked cyt *c* binding to BLM_{DMPC}/SAM_{COOH} (**Figure S3**). Although the BLM_{DMPC} formed on SAM_{COOH} in the absence of C*c*O, no adsorption of cyt *c* to BLM_{DMPC}/SAM_{COOH} occurred because no positive increase of amide I' and II' bands was observed during the cyt *c* binding process. In contrast, cyt *c* was adsorbed to SAM_{COOH} in the absence of BLM_{DMPC} (**Figure S4**). These control experiments suggest that no adsorption of cyt *c* occurs on BLM_{DMPC}, supporting that cyt *c* can be attached to the cyt *c* binding site of C*c*O of ptBLM/SAM_{COOH} but highly unlikely to BLM_{DMPC}.

The ptBLM formation process was also tracked by electrochemical impedance spectroscopy (EIS). To exclude effects of the model used for EIS data analysis, capacitances were estimated by reading out the diameter of the first semicircle of the frequency-weighted Cole–Cole plots at high frequencies (**Figure S5**) because the first half semicircle describes the capacitive behavior of the entire SAM or BLM.[29-30] Capacitances tend to decrease in the following order: SAM_{COOH} (5.8 μF cm^{-2}) > C*c*O/SAM_{COOH} (4.1 μF cm^{-2}) > BLM_{DMPC}-C*c*O/SAM_{COOH} (1.5 μF cm^{-2}). The value for BLM_{DMPC}-C*c*O/SAM_{COOH} is lower than that of C*c*O/SAM_{COOH}, indicating the formation of ptBLM. This can be rationalized based on higher dielectric constants of embedded membrane proteins (ε ~ 2-40), compared with the hydrophobic core of the phospholipid ($\varepsilon \sim 2$).[30] The absolute value of the capacitance of BLM_{DMPC}-C*c*O/SAM_{COOH} indicates the formation of the single-layered ptBLM.

To understand the electrocatalytic activity of C*c*O for the ORR, cyclic voltammograms (CVs) of C*c*O/SAM_{COOH}/Au and C*c*O/SAM_{OH}/Au before the cyt *c* binding were recorded and cathodic currents were observed under oxygen but not under Ar (**Figure 4c** and **4d**). The cathodic currents

observed under oxygen are associated with the enzymatic activity of C*c*O for the ORR.[11,13,31] C*c*O is believed to show the anti-cooperative redox behavior: the reduction of one heme inhibits the reduction of the other.[10] The first electron shows an equal affinity for heme *a* and a_3. For bovine C*c*O at pH 7, the first reduction process is reported to occur at 0.34 V vs. SHE between the fully oxidized $a^{3+}a_3{}^{3+}$ and the half-reduced state, which is a mixture of the $a^{2+}a_3{}^{3+}$ and $a^{3+}a_3{}^{2+}$, and then the second and the third reduction processes occur at 0.26 and 0.19 V vs. SHE, respectively,[10,32-33] where a copper center is likely involved as the third redox site.

The binding of cyt *c* to BLM_{DMPC}-C*c*O/SAM_{COOH}/Au increases cathodic currents for the ORR (**Figure 4c**): BLM_{DMPC}-C*c*O/SAM_{COOH}/Au before and after the cyt *c* binding showed current densities of –0.88 and –1.12 μA cm^{-2} at –0.1 V vs. SHE for the ORR, respectively. Based on these current densities, a factor of 1.3 enhancement for the electrocatalytic ORR was obtained for the cyt *c* binding to BLM_{DMPC}-C*c*O/SAM_{COOH}/Au. In contrast, no such enhancement was observed for BLM_{DMPC}-C*c*O/SAM_{OH}/Au (**Figure 4d**). These results imply that the cyt *c*–C*c*O protein–protein interaction could affect protein structures and the interfacial electron transfer from the Au electrode to the binuclear active site of heme a_3 and Cu_B of C*c*O *via* electron tunneling because the binuclear active site is placed near the electrode surface for C*c*O/SAM_{COOH}/Au.

To understand protein–lipid interactions in detail, we also tracked the formation of BLM of DPPC (BLM_{DPPC}) on C*c*O/SAM_{COOH}/Au and then the cyt *c* binding by SEIRA spectroscopy. We observed the increase of the negative ν(OH) band and positive $\nu_s(CH_2)$ and $\nu_{as}(CH_2)$ bands (**Figure 5a** and **5b**), which are similar to the BLM_{DMPC} formation on C*c*O/SAM_{COOH}/Au (**Figure 3a** and **5b**). The peak position of $\nu_{as}(CH_2)$ for BLM_{DPPC} was found at 2919 cm^{-1} (**Figure 5b**), which is lower than that for BLM_{DMPC}-C*c*O/SAM_{COOH}/Au (2923 cm^{-1}) (**Figure 3b**), as mentioned above. The $\nu_{as}(CH_2)$ band position for BLM_{DPPC} is close to that of the well-ordered alkyl chains (2918

cm^{-1}).[34] The $\nu_{as}(CH_2)$ peak position is related to the average number of *gauche* conformers in hydrocarbon chains and the wavenumber of $\nu_{as}(CH_2)$ increases with increasing the number of the *gauche* conformers.[17,35] Thus, ptBLM$_{DPPC}$ is more densely packed than ptBLM$_{DMPC}$. This can be caused by the difference in chain length: DPPC has acyl chains 16 carbon-atoms long whereas DMPC has acyl chains 14 carbon-atoms long (**Figure 1**). This difference leads to the formation of the densely packed BLM$_{DPPC}$.[36]

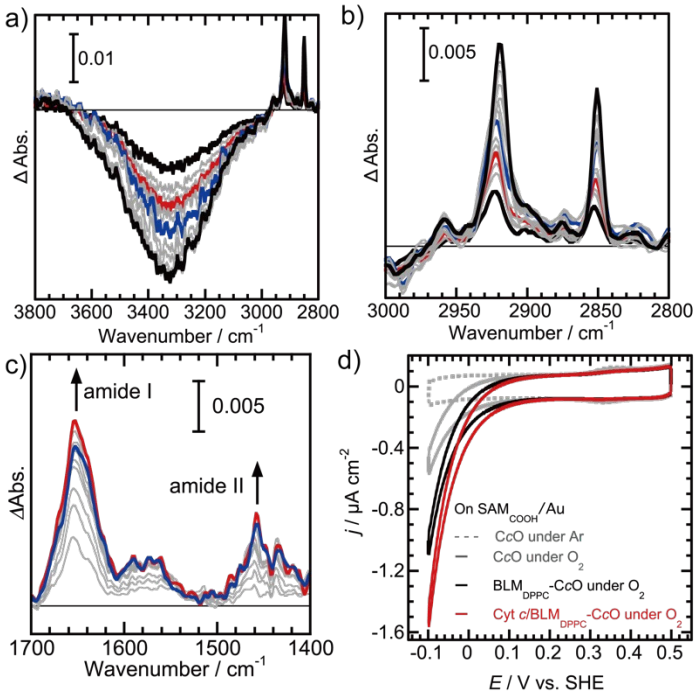

Figure 5. SEIRA spectral changes during (a,b) the BLM$_{DPPC}$ formation on C*c*O/SAM$_{COOH}$/Au in a 50 mM phosphate-buffered solution (pH 6.5). A polarization-modulated SEIRA spectrum recorded just after the addition of DPPC solution at t = 0 min was used as the reference spectrum. The SEIRA spectra in black indicate the spectra at t = 22 and 247 min. The SEIRA spectra in red and blue show the spectra at t = 67 and 112 min after the addition of bio-beads at t = 60 and 100 min, respectively. (c) SEIRA spectral changes during cyt *c* binding to BLM$_{DPPC}$-C*c*O/SAM$_{COOH}$/Au in a 50 mM phosphate-buffered D_2O solution (pD 6.5). A polarization-modulated spectrum recorded in the phosphate-buffered D_2O solution before the addition of cyt *c* was used as the reference spectrum (t = 0 min). The traces in red indicate SEIRA spectra recorded at t = 127 min. The traces in blue indicate the spectra collected after rinsing the electrode surface with the buffered solution. (d) CVs recorded at 10 mV s^{-1} in a 50 mM phosphate-buffered aqueous solution (pH 6.5) for BLM$_{DPPC}$-C*c*O/SAM$_{COOH}$/Au before and after the cyt *c* binding. The

electrodes were prepared step by step as follows: C*c*O/SAM_{COOH}/Au, BLM_{DPPC}-C*c*O/SAM_{COOH}/Au and then cyt *c*/BLM_{DPPC}-C*c*O/SAM_{COOH}/Au for (d).

For $ptBLM_{DPPC}$, the addition of cyt *c* into the phosphate-buffered D_2O solution initiated an increase of positive amide I' and II' bands (**Figure 5c**). Since these bands remained even after rinsing the electrode with the buffered solution, cyt *c* can be attached to $ptBLM_{DPPC}$ on SAM_{COOH}. CVs of BLM_{DPPC}-C*c*O/SAM_{COOH}/Au showed the cathodic currents under oxygen (**Figure 5d**). The cyt *c*-BLM_{DPPC}-C*c*O/SAM_{COOH}/Au gave a cathodic current density of –1.53 μA cm^{-2} at –0.1 V vs. SHE under oxygen whereas C*c*O/SAM_{COOH}/Au in the absence of DPPC and cyt *c* showed –0.55 μA cm^{-2} (**Figure 5d**). These current densities enable us to calculate an enhancement factor of 2.8, caused by the $ptBLM_{DPPC}$ formation and the cyt *c* binding. This enhancement factor is higher than a factor of 2.0 obtained for the cyt *c*-$ptBLM_{DMPC}$ electrode from the comparison between current densities of –1.22 μA cm^{-2} for cyt *c*-BLM_{DMPC}-C*c*O/SAM_{COOH}/Au and –0.57 μA cm^{-2} for C*c*O/SAM_{COOH}/Au (**Figure 4d**). The difference in the enhancement factor indicates that the cyt *c* binding to the densely packed $ptBLM_{DPPC}$ could increase the electrocatalytic C*c*O activity for the ORR. The BLM packing density can affect the interfacial resistance for oxygen permeability and/or oxygen solubility in BLMs,[4,8,37-39] resulting in the improvement of the ORR activity of C*c*O in ptBLMs.

In summary, we immobilized bovine C*c*O on SEIRA-active Au electrodes *via* mixed SAMs, reconstituted ptBLMs of phospholipids, and then attached cyt *c* to the ptBLMs. Each step was tracked by SEIRA spectroscopy and the effect of interfacial interactions on the enzymatic activity of C*c*O was investigated by PFE. The cyt *c* binding site of C*c*O on SAM_{COOH} is directed away

from the electrode substrate pointing to the solution whereas it on SAM_{OH} is directed to the electrode substrate. C*c*O immobilized on SAM_{COOH} electrostatically interacts with cyt *c* but it does not on SAM_{OH}. Since the cyt *c* binding increased the enzymatic activity of C*c*O in the ptBLM, protein–protein interactions between cyt *c* and C*c*O can modulate its catalytic activity. SEIRA spectra for the BLM formation indicate that DPPC forms more densely packed BLMs than DMPC in ptBLMs of C*c*O. The ptBLM with DPPC showed higher electrocatalytic activity for the ORR than that with DMPC. Thus, protein–lipid interactions in ptBLMs also modulate the enzymatic activity.

This work demonstrates that PFE coupled with SEIRA spectroscopy is a powerful analytical technique to understand impacts of interfacial interactions of membrane proteins with biomolecules including water-soluble proteins and phospholipids on the protein functionality in ptBLMs. This technique would enable us to gain mechanistic insights into protein dynamics, functionality and synchronization at bio-membrane interfaces involving protein-protein and protein-lipid interactions and encourage us to develop electrocatalysts [40-41] and electrochemical devises including bio-fuel cells and biosensors.[42-43]

ASSOCIATED CONTENT

Supporting Information.

The following files are available free of charge.

Experimental details, SEIRA spectral changes during cyt *c* binding to C*c*O/SAM_{COOH}/Au, C*c*O/SAM_{OH}/Au, BLM_{DMPC}/SAM_{COOH}/Au and SAM_{COOH}/Au, and EIS data (PDF)

AUTHOR INFORMATION

Notes

The authors declare no competing financial interests.

ACKNOWLEDGMENT

The authors thank Dr. Minoru Kubo (University of Hyogo) for his fruitful discussion on C*c*O and Shingo Mukai, Yusuke Kawamura, Katsuhisa Ishikawa and Takahiko Hasegawa (Technical Division, Institute for Catalysis, Hokkaido University) for their technical supports on the experimental setup for the SEIRA spectroscopy. This work was supported by JSPS KAKENHI Grant numbers JP16K20882, JP21K05124 (to M.K.), and JP19H02664 (to I.Y.), Hokkaido University through Program for Leading Graduate Schools (Hokkaido University "Ambitious Leader's Program") (to S.O.), and a MEXT Program for Development of Environmental Technology using Nanotechnology from the Ministry of Education, Culture, Sports, Science and Technology, Japan.

REFERENCES

(1) Hayashi, T.; Asano, Y.; Shintani, Y.; Aoyama, H.; Kioka, H.; Tsukamoto, O.; Hikita, M.; Shinzawa-Itoh, K.; Takafuji, K.; Higo, S.; Kato, H.; Yamazaki, S.; Matsuoka, K.; Nakano, A.; Asanuma, H.; Asakura, M.; Minamino, T.; Goto, Y.-i.; Ogura, T.; Kitakaze, M.; Komuro, I.; Sakata, Y.; Tsukihara, T.; Yoshikawa, S.; Takashima, S. *Higd1a* is a positive regulator of cytochrome *c* oxidase. *Proc. Natl. Acad. Sci. U.S.A.* **2015,** *112*, 1553-1558.
(2) Nagao, T.; Shintani, Y.; Hayashi, T.; Kioka, H.; Kato, H.; Nishida, Y.; Yamazaki, S.; Tsukamoto, O.; Yashirogi, S.; Yazawa, I.; Asano, Y.; Shinzawa-Itoh, K.; Imamura, H.; Suzuki, T.; Suzuki, T.; Goto, Y.-i.; Takashima, S. Higd1a improves respiratory function in the models of mitochondrial disorder. *FASEB J.* **2020,** *34*, 1859-1871.
(3) Hirst, J. Open questions: respiratory chain supercomplexes—why are they there and what do they do? *BMC Biol.* **2018,** *16*, 111.
(4) Wikström, M.; Krab, K.; Sharma, V. Oxygen Activation and Energy Conservation by Cytochrome c Oxidase. *Chem. Rev.* **2018,** *118*, 2469-2490.
(5) Pelster, L. N.; Minteer, S. D. Mitochondrial Inner Membrane Biomimic for the Investigation of Electron Transport Chain Supercomplex Bioelectrocatalysis. *ACS Catal.* **2016,** *6*, 4995-4999.
(6) Shimada, S.; Shinzawa-Itoh, K.; Baba, J.; Aoe, S.; Shimada, A.; Yamashita, E.; Kang, J.; Tateno, M.; Yoshikawa, S.; Tsukihara, T. Complex structure of cytochrome c–cytochrome c oxidase reveals a novel protein–protein interaction mode. *EMBO J.* **2017,** *36*, 291-300.
(7) Liko, I.; Degiacomi, M. T.; Mohammed, S.; Yoshikawa, S.; Schmidt, C.; Robinson, C. V. Dimer interface of bovine cytochrome *c* oxidase is influenced by local posttranslational modifications and lipid binding. *Proc. Natl. Acad. Sci. U.S.A.* **2016,** *113*, 8230-8235.
(8) Shinzawa-Itoh, K.; Aoyama, H.; Muramoto, K.; Terada, H.; Kurauchi, T.; Tadehara, Y.; Yamasaki, A.; Sugimura, T.; Kurono, S.; Tsujimoto, K.; Mizushima, T.; Yamashita, E.; Tsukihara, T.; Yoshikawa, S. Structures and physiological roles of 13 integral lipids of bovine heart cytochrome *c* oxidase. *EMBO J.* **2007,** *26*, 1713-1725.
(9) Tsukihara, T.; Aoyama, H.; Yamashita, E.; Tomizaki, T.; Yamaguchi, H.; Shinzawa-Itoh, K.; Nakashima, R.; Yaono, R.; Yoshikawa, S. The Whole Structure of the 13-Subunit Oxidized Cytochrome c Oxidase at 2.8 &#xc5. *Science* **1996,** *272*, 1136-1144.
(10) Melin, F.; Hellwig, P. Redox Properties of the Membrane Proteins from the Respiratory Chain. *Chem. Rev.* **2020,** *120*, 10244-10297.
(11) Wang, X.; Clément, R.; Roger, M.; Bauzan, M.; Mazurenko, I.; Poulpiquet, A. d.; Ilbert, M.; Lojou, E. Bacterial Respiratory Chain Diversity Reveals a Cytochrome c Oxidase Reducing O2 at Low Overpotentials. *J. Am. Chem. Soc.* **2019,** *141*, 11093-11102.
(12) Li, J.; Cheng, G.; Dong, S. Direct electron transfer to cytochrome c oxidase in self-assembled monolayers on gold electrodes. *J. Electroanal. Chem.* **1996,** *416*, 97-104.
(13) Meyer, T.; Melin, F.; Xie, H.; von der Hocht, I.; Choi, S. K.; Noor, M. R.; Michel, H.; Gennis, R. B.; Soulimane, T.; Hellwig, P. Evidence for Distinct Electron Transfer Processes in Terminal Oxidases from Different Origin by Means of Protein Film Voltammetry. *J. Am. Chem. Soc.* **2014,** *136*, 10854-10857.
(14) Haas, A. S.; Pilloud, D. L.; Reddy, K. S.; Babcock, G. T.; Moser, C. C.; Blasie, J. K.; Dutton, P. L. Cytochrome c and Cytochrome *c* Oxidase: Monolayer Assemblies and Catalysis. *J. Phys. Chem. B* **2001,** *105*, 11351-11362.
(15) Ataka, K.; Giess, F.; Knoll, W.; Naumann, R.; Haber-Pohlmeier, S.; Richter, B.; Heberle, J. Oriented Attachment and Membrane Reconstitution of His-Tagged Cytochrome c Oxidase to a

Gold Electrode: In Situ Monitoring by Surface-Enhanced Infrared Absorption Spectroscopy. *J. Am. Chem. Soc.* **2004,** *126*, 16199-16206.
(16) Ataka, K.; Richter, B.; Heberle, J. Orientational Control of the Physiological Reaction of Cytochrome c Oxidase Tethered to a Gold Electrode. *J. Phys. Chem. B* **2006,** *110*, 9339-9347.
(17) Kato, M.; Masuda, Y.; Yoshida, N.; Tosha, T.; Shiro, Y.; Yagi, I. Impact of membrane protein-lipid interactions on formation of bilayer lipid membranes on SAM-modified gold electrode. *Electrochim. Acta* **2021,** *373*, 137888.
(18) Stripp, S. T. In Situ Infrared Spectroscopy for the Analysis of Gas-processing Metalloenzymes. *ACS Catal.* **2021,** *11*, 7845-7862.
(19) Kruse, F.; Nguyen, A. D.; Dragelj, J.; Schlesinger, R.; Heberle, J.; Mroginski, M. A.; Weidinger, I. M. Characterisation of the Cyanate Inhibited State of Cytochrome c Oxidase. *Sci. Rep.* **2020,** *10*, 3863.
(20) Kato, M.; Nakagawa, S.; Tosha, T.; Shiro, Y.; Masuda, Y.; Nakata, K.; Yagi, I. Surface-Enhanced Infrared Absorption Spectroscopy of Bacterial Nitric Oxide Reductase under Electrochemical Control Using a Vibrational Probe of Carbon Monoxide. *J. Phys. Chem. Lett.* **2018,** *9*, 5196-5200.
(21) Kato, M.; Cardona, T.; Rutherford, A. W.; Reisner, E. Covalent Immobilization of Oriented Photosystem II on a Nanostructured Electrode for Solar Water Oxidation. *J. Am. Chem. Soc.* **2013,** *135*, 10610-10613.
(22) Barth, A. Infrared spectroscopy of proteins. *Biochim. Biophys. Acta –Bioenergetics* **2007,** *1767*, 1073-1101.
(23) Okuno, D.; Iwase, T.; Shinzawa-Itoh, K.; Yoshikawa, S.; Kitagawa, T. FTIR Detection of Protonation/Deprotonation of Key Carboxyl Side Chains Caused by Redox Change of the CuA-Heme a Moiety and Ligand Dissociation from the Heme a3-CuB Center of Bovine Heart Cytochrome *c* Oxidase. *J. Am. Chem. Soc.* **2003,** *125*, 7209-7218.
(24) Ataka, K.; Stripp, S. T.; Heberle, J. Surface-enhanced infrared absorption spectroscopy (SEIRAS) to probe monolayers of membrane proteins. *Biochim. Biophys. Acta – Biomembranes* **2013,** *1828*, 2283-2293.
(25) Jiang, X.; Zaitseva, E.; Schmidt, M.; Siebert, F.; Engelhard, M.; Schlesinger, R.; Ataka, K.; Vogel, R.; Heberle, J. Resolving voltage-dependent structural changes of a membrane photoreceptor by surface-enhanced IR difference spectroscopy. *Proc. Natl. Acad. Sci. U.S.A.* **2008,** *105*, 12113-12117.
(26) Kadenbach, B.; Huttemann, M. The subunit composition and function of mammalian cytochrome c oxidase. *Mitochondrion* **2015,** *24*, 64-76.
(27) Friedrich, M. G.; Gieβ, F.; Naumann, R.; Knoll, W.; Ataka, K.; Heberle, J.; Hrabakova, J.; Murgida, D. H.; Hildebrandt, P. Active site structure and redox processes of cytochrome *c* oxidase immobilised in a novel biomimetic lipid membrane on an electrode. *Chem. Commun.* **2004**, 10.1039/B410998H, 2376-2377.
(28) Uchida, T.; Osawa, M.; Lipkowski, J. SEIRAS studies of water structure at the gold electrode surface in the presence of supported lipid bilayer. *J. Electroanal. Chem.* **2014,** *716*, 112-119.
(29) Jeuken, L. J. C.; Daskalakis, N. N.; Han, X.; Sheikh, K.; Erbe, A.; Bushby, R. J.; Evans, S. D. Phase separation in mixed self-assembled monolayers and its effect on biomimetic membranes. *Sens. Actuators B* **2007,** *124*, 501-509.

(30) Wiebalck, S.; Kozuch, J.; Forbrig, E.; Tzschucke, C. C.; Jeuken, L. J. C.; Hildebrandt, P. Monitoring the Transmembrane Proton Gradient Generated by Cytochrome bo3 in Tethered Bilayer Lipid Membranes Using SEIRA Spectroscopy. *J. Phys. Chem. B* **2016,** *120*, 2249-2256.
(31) Melin, F.; Hellwig, P. Recent advances in the electrochemistry and spectroelectrochemistry of membrane proteins. *Biol. Chem.* **2013,** *394*, 593-609.
(32) Reddy, K. V.; Hendler, R. W.; Bunow, B. Complete analysis of the cytochrome components of beef heart mitochondria in terms of spectra and redox properties. Cytochromes aa3. *Biophys. J.* **1986,** *49*, 705-715.
(33) Hendler, R. W.; Reddy, K. V.; Shrager, R. I.; Caughey, W. S. Analysis of the spectra and redox properties of pure cytochromes aa3. *Biophys. J.* **1986,** *49*, 717-729.
(34) Quirk, A.; Lardner, M. J.; Tun, Z.; Burgess, I. J. Surface-Enhanced Infrared Spectroscopy and Neutron Reflectivity Studies of Ubiquinone in Hybrid Bilayer Membranes under Potential Control. *Langmuir* **2016,** *32*, 2225-2235.
(35) Jemmett, P. N.; Milan, D. C.; Nichols, R. J.; Cox, L. R.; Horswell, S. L. Effect of Molecular Structure on Electrochemical Phase Behavior of Phospholipid Bilayers on Au(111). *Langmuir* **2021,** *37*, 11887-11899.
(36) Higgins, M. J.; Polcik, M.; Fukuma, T.; Sader, J. E.; Nakayama, Y.; Jarvis, S. P. Structured Water Layers Adjacent to Biological Membranes. *Biophys. J.* **2006,** *91*, 2532-2542.
(37) Cordeiro, R. M. Reactive oxygen species at phospholipid bilayers: Distribution, mobility and permeation. *Biochim. Biophys. Acta – Biomembranes* **2014,** *1838*, 438-444.
(38) Möller, M. N.; Li, Q.; Chinnaraj, M.; Cheung, H. C.; Lancaster, J. R.; Denicola, A. Solubility and diffusion of oxygen in phospholipid membranes. *Biochim. Biophys. Acta – Biomembranes* **2016,** *1858*, 2923-2930.
(39) Al-Abdul-Wahid, M. S.; Evanics, F.; Prosser, R. S. Dioxygen Transmembrane Distributions and Partitioning Thermodynamics in Lipid Bilayers and Micelles. *Biochemistry* **2011,** *50*, 3975-3983.
(40) Kato, M.; Yagi, I. Electrocatalytic Oxygen Reduction at Multinuclear Metal Active Sites Inspired by Metalloenzymes. *e-J. Surf. Sci. Nanotechnol.* **2020,** *18*, 81-93.
(41) Kato, M.; Fujibayashi, N.; Abe, D.; Matsubara, N.; Yasuda, S.; Yagi, I. Impact of Heterometallic Cooperativity of Iron and Copper Active Sites on Electrocatalytic Oxygen Reduction Kinetics. *ACS Catal.* **2021,** *11*, 2356-2365.
(42) Manickam, P.; Kaushik, A.; Karunakaran, C.; Bhansali, S. Recent advances in cytochrome *c* biosensing technologies. *Biosens. Bioelectron.* **2017,** *87*, 654-668.
(43) Ashe, D.; Alleyne, T.; Iwuoha, E. Serum cytochrome c detection using a cytochrome *c* oxidase biosensor. *Biotechnol. Appl. Biochem.* **2007,** *46*, 185-189.